Laser–Electron Conversion Efficiency at Intensities Greater than 10^{19} W/cm^2

K. B. Wharton
B. Hammel
S. Hatchett
*C. Joshi**
M. Key
J. Moody
A. A. Offenberger
M. Perry
S. C. Wilks
V. Yanovsky

Introduction

Experimental investigation of plasma phenomena in ultraintense laser fields, in which electrons oscillate at relativistic velocities, has recently become possible with the advent of multiterawatt, short-pulse lasers. Several mechanisms that can transfer laser energy to the plasma electrons have been described.[1] One proposed application for such energetic electrons is sparking a fusion reaction in the fast-ignitor scheme.[2] Crucial, but unresolved, issues include the conversion efficiency of laser energy to electron energy, electron directionality, and temperature or mean energy of the electrons. We present the first measurements of the full, forward-hemisphere, laser-to-electron conversion efficiency, directionality, and mean electron energy in laser–solid interactions at incident laser intensities of 2 to 4×10^{19} W/cm^2. Such parameters will help determine the feasibility of the fast ignitor scheme in future laser facilities, such the National Ignition Facility.

One mechanism for collisionless laser–electron coupling in a plasma is the $-e\,\mathbf{v} \times \mathbf{B}$ Lorentz force on electrons oscillating in the electromagnetic field of a high-intensity laser. When the laser fields terminate at a critical-density surface, this force can ponderomotively accelerate electrons in the direction of laser propagation.[3] Other collisionless laser–electron coupling mechanisms at the critical density include resonance absorption,[4] parametric instabilities,[5] and vacuum heating.[6] Coupling at subcritical densities associated with the excitation of electron plasma waves can also accelerate plasma electrons.[7] Previous experiments have measured laser-accelerated electrons at lower intensities.[8–14] One recent experiment using strongly relativistic intensities ($I\lambda^2 > 10^{19}$ W cm^{-2} μm^2) measured high-energy electrons in vacuum after leaving a foil target in which they were produced.[15]

Experimental Configuration

Our experiments were performed at the Nova laser facility at Lawrence Livermore National Laboratory (LLNL) on a beamline that uses chirped-pulse amplification.[16] This short-pulse system supplies 12 to 30 J of 1.06-μm light in 400 fs. The peak intensity is 10^7 times greater than the amplified spontaneous emission (ASE), which begins about 3 ns before the main pulse. An additional 400-fs prepulse, reaching ~10^{-3} of the peak intensity, arrives ~2 ns early. The final focusing optic is an $f/3$ off-axis parabola, which produces a measured 15-μm full-width-at-half-maximum (FWHM) focal spot (peak intensity of 4×10^{19} W/cm^2 for 30 J). Measurements[17] and simulations show that the ASE and prepulse create an underdense plasma in front of the target with a scale length on the order of 10 μm. In this plasma, the intense laser may experience further self-focusing.[18,19]

Both the temperature and absolute number of the laser-produced electrons were characterized by detecting the electron-induced K_α x-ray emission from buried layers in multilayer targets, which is a well established technique.[8–12,14] This is an indirect method for measuring electrons before they leave the target via the inner-shell ionization of a tracer material at a known depth in the target. By varying the depth of the tracer layer, an electron spectrum can be inferred from the corresponding change in the K_α x-ray yield.

*University of California at Los Angeles, Los Angeles, CA

In the experiment, P-polarized laser light was incident at 25° to the target normal. The front (laser-incident) layer of the target was a 6- × 8-mm rectangular foil of various materials (CH, Al, or Cu) with a mass per unit area ranging from 0.02 to 0.45 g/cm^2. The middle layer of the target was a smaller (5- × 7-mm) foil of 50-μm-thick Mo. Electrons produced in the front layer transported into this Mo layer, knocking out inner-shell electrons and creating 17.5-keV K_α x rays. Finally, a layer of 1-mm-thick CH (6 × 8 mm) covered the back of the target, which protected the Mo layer from electrons that might return to the target (those pulled back by electrostatic forces). This CH layer stopped electrons with energies less than 300 keV (550-keV attenuation for a double pass), but had a negligible effect on the 17.5-keV x rays. We found that this layer lowered the Mo K_α x-ray signal by a factor of ~2, indicating that most of the K_α radiation was produced by electrons, not x rays.

We chose Mo for our tracer material so that the characteristic 17.5-keV K_α photon energy would be significantly greater than that of the x rays produced by the thermal plasma around the laser focus. This is important for avoiding photopumping of the K_α x-ray line.[8] Spectroscopic measurements of an Al layer buried under a very thin layer of 5-μm CH showed a thermal plasma temperature of 300 to 600 eV in separate experiments with the same laser.[20] Further evidence that thermal x rays were unimportant was that the 20- to 30-keV x-ray spectrum was very similar from both the front and back of pure Al and Cu targets, which were optically thick in this energy range. This result signified that these x rays were predominantly bremsstrahlung photons produced throughout the cold target.

K_α x rays from the Mo layer were detected by a 16-bit, charged-coupled-device (CCD) detector situated 2.16 m from the target and 45° from the rear target normal. The CCD was filtered with 75 μm of Sn, limiting the x-ray flux and making it unlikely that two high-energy photons would be absorbed in the same pixel. The counts recorded on each pixel were proportional to the x-ray photon energy. We performed a statistical analysis on each set of data to determine what fraction of the signal was obscured by double hits due to the lower-energy x-ray continuum.

The CCD camera was absolutely calibrated with a Cd-109 (22-keV) source at two different occasions during the experiments. The two calibrations agreed to within 3% and allowed us to calculate the number of incident x rays from the measured hits on the camera. To scale the 22-keV calibration energy to the 17.5-keV K_α x rays, we assumed that the detector response was proportional to the absorption of the 14-μm-thick Si CCD chip.

Theoretical Analysis

The many possible electron trajectories in the target made a comprehensive analytical description difficult. Instead, we used the electron–photon transport Monte Carlo code ITS to interpret the data.[21] The output of the ITS code was the number of K_α x rays per steradian emitted from a given target in the detector direction, normalized to the number of source electrons. In addition to calculating electron transport and ionization, ITS also computed the x-ray continuum produced by bremsstrahlung of fast electrons and the resulting photoionization of Mo atoms. The photopumped K_α x rays were typically 10% of the total.

We assumed that the electron source has the form of a Maxwellian energy distribution, which has been seen in particle-in-cell simulations[3,19] and in experiments.[11,15] However, because there is no intrinsic reason for the electrons to be Maxwellian, we also ran ITS simulations of other possible distributions. For a relativistic Maxwellian, the mean electron energy E_0 ranges from $3/2\ kT$ (nonrelativistic electrons) to $3\ kT$ (highly relativistic electrons). We compared this to the case of a purely exponential spectrum $f(E) = \exp(-E/kT)$, for which $E_0 = kT$. The ITS results were entirely consistent to within 10% for these different spectra, provided that E_0 (not kT) was kept constant. This demonstrated that our technique is not sensitive to the tail of the electron distribution (the slope of which determines kT), but rather to the mean-energy bulk of the distribution. For this reason, our results are not directly comparable to some previous measurements of bremsstrahlung x rays or the high-energy electron tail.[15] However, our technique is appropriate for measurements of absolute conversion efficiency, which depend on the mean energy E_0.

One assumption required in ITS concerns the cone angle of the electrons. For now, we assume that the electrons spray forward isotropically from the laser focus into a full hemisphere; we further discuss this assumption later. ITS also assumes that the electrons transport through cold material, and the code ignores collective effects, such as self-consistent magnetic[19,22] and electrostatic[23–25] fields. Because of the complexity of the physics involved, our use of ITS is not intended to fully model the experiment, but is used as a benchmark for interpreting the data.

Results

Figure 1 shows the Mo K_α yields from the targets with Al front layers, along with the best fits from the ITS code. The slope of the data (on a log plot) is sensitive to the mean energy E_0 of the electrons, whereas the absolute magnitude yields the laser-to-electron

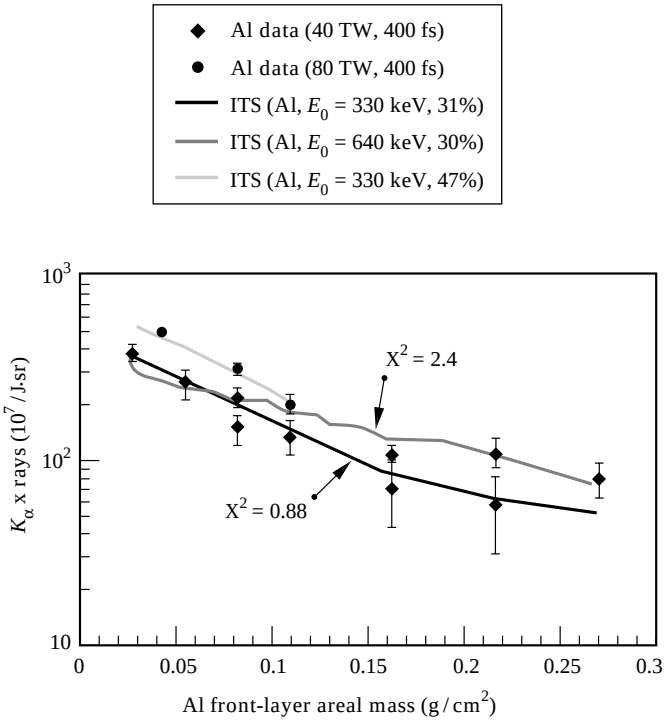

FIGURE 1. K_α signal from Al targets, in units of 10^7 x rays per incident joule and per steradian, vs areal mass of Al front layer of the target. Diamonds are experimental data at intensities of 4×10^{19} W/cm^2; circles are data at 2×10^{19} W/cm^2. The ITS fits are listed by average energy E_0 and conversion efficiency η (in percent); some X^2 fit parameters are shown. All values of η are multiplied by 0.7 if the electrons are assumed to be directed in a 30° half-angle cone. (08-00-0598-1209pb01)

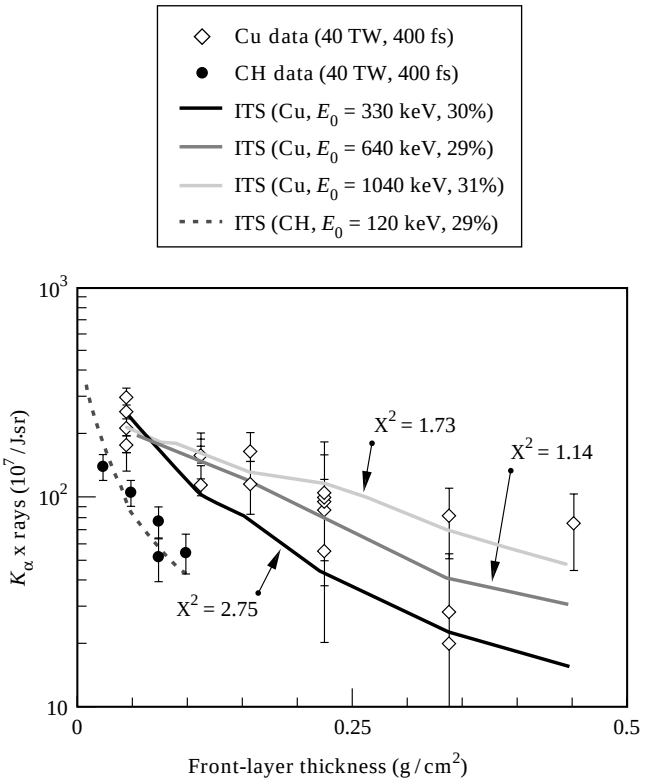

FIGURE 2. K_α signal from the target, with the same units as in Figure 1. Circles are data from CH front-layer targets; diamonds are data from Cu targets, both at 2×10^{19} W/cm^2. The ITS fits are listed by average energy E_0 and conversion efficiency η (in percent); some X^2 fit parameters are shown. All values of η are multiplied by 0.7 if the electrons are assumed to be directed in a 30° half-angle cone. (08-00-0598-1210pb01)

conversion efficiency η. Error bars were computed from a combination of counting errors and fluctuations in the background x-ray noise.

We fit the data with a series of ITS runs, which computed the K_α x-ray yield as a function of the transport-layer thickness for a given electron mean energy E_0, and then found the conversion efficiency η that minimized the chi-squared (X^2) per degree of freedom. The data at an intensity of 2×10^{19} W/cm^2 are fit by an ITS run with $E_0 = 330$ keV ($kT = 170$ keV) and η = 31%. For this fit, the X^2 is reasonably small (0.88). An ITS run for $E_0 = 640$ keV ($kT = 300$ keV) is also shown, although the X^2 of this fit is much larger (2.4). Three data points at an intensity of 4×10^{19} W/cm^2 show a greater η (47%), but roughly the same mean energy.

Figure 2 shows the experimental results for CH and Cu targets at a laser intensity of 2×10^{19} W/cm^2. The CH targets produced the smallest signal, corresponding to $E_0 = 120$ keV and η = 29%. The Cu data have the largest error bars, due to higher x-ray noise, but are best fit by $E_0 = 640$ keV and η = 29%. Higher and lower energy fits to the Cu data are shown as well. The lower-intensity Al data from Figure 1 are at the same intensity, namely 2×10^{19} W/cm^2; recall that these data were fit by $E_0 = 330$ keV and η = 31%. The data show a change of mean electron energy with target material, although the conversion efficiencies remain roughly constant.

Electron Cone-Angle Measurements

The assumption that electrons are spraying into a full hemisphere might artificially increase the apparent conversion efficiency. To measure the directionality of electrons, a stainless-steel razor blade 750 μm thick was placed between the back of the target and the CCD detector, creating a 1D penumbral image of the x-ray source on the CCD.[11,26] Using this configuration, 2×10^{19} W/cm^2 laser pulses were shot at some of the previously

described targets: CH front layers (varied thicknesses), Mo middle layers, and optional CH back layers to prevent electron double hits. The lack of measured x rays above 6 keV from pure CH targets, along with the opacity of the razor blade to x rays under 25 keV, meant that the size of the 6- to 25-keV x-ray source was a good measure of where the electron beam intersected the Mo layer. Varying the depth of the Mo gave us an estimate of the electron cone angle.

Figure 3 shows the measured spot size of the x-ray source plotted against the buried depth of the 50-μm Mo layer and compares these values to ITS calculations of the predicted measurements for electron beams with 30° and 90° half-cone angles. The large error bars result from the derivative that is required to extract the spot size from the data. For Mo layers buried 100 to 250 μm into the target, the data roughly corresponds to an electron cone half-angle of 90°, a full hemisphere. However, for the thicker targets, the x-ray source corresponds closer to an electron beam of a 30° half-cone angle. Although the error bars are large, these data suggest some beaming of high-energy electrons (>200 keV) that penetrate through the thicker targets. The bulk of the lower-energy electrons seem to be spraying into a full hemisphere. Using ITS to recalculate the conversion efficiencies based on a 30° half-angle electron source lowers η to 0.7 of the 90° values given above. The mean electron energies were not affected.

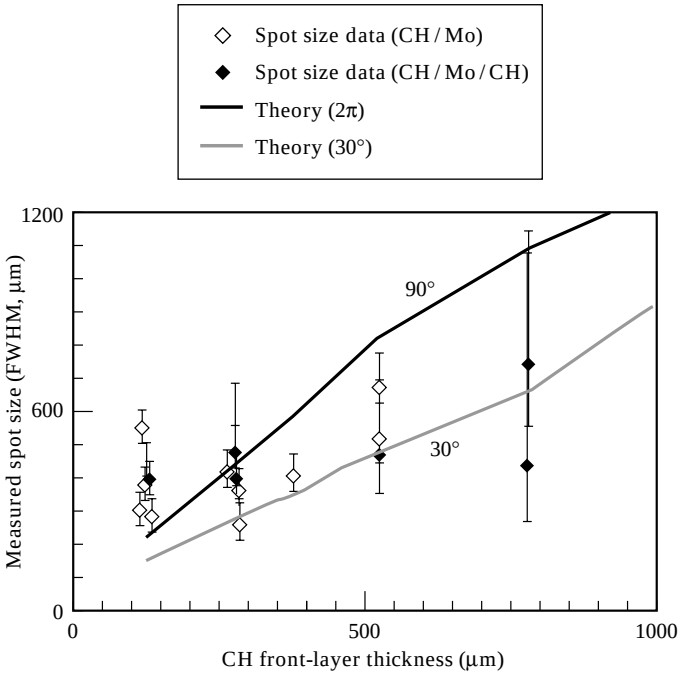

FIGURE 3. Measured size (FWHM in μm) of the x-ray source plotted against thickness (μm) of the front CH layer. Open diamonds are from targets with a back layer of 1-mm CH; solid diamonds had no CH back layer. The black line is an ITS fit of the expected results from an unbeamed electron source (90° half angle). The gray line is an ITS simulation of an electron source with a 30° half angle. (08-00-0598-1181pb01)

Applying this beaming effect to the earlier data, our measurements correspond to $\eta = 21\% \pm 5\%$ for all materials at a laser intensity of 2×10^{19} W/cm^2, and $\eta = 33\% \pm 5\%$ for the high-intensity (4×10^{19} W/cm^2) shots on Al targets.

Discussion

The measurements of average energy seem to vary with target material rather than intensity. Our data shows that Cu-produced electrons are the most penetrating, although the error bars on the measurements still allow the possibility that the Al and Cu spectra could be equivalent. The CH electrons are less penetrating and apparently colder, although they seem to have roughly the same conversion efficiency as that for the Al and Cu targets. The conversion efficiency in CH, however, has an additional systematic error because the range of an $E_0 = 120$-keV electron is smaller than the typical target thickness, which means that in CH we are not measuring the bulk of the electron distribution as we do in Al and Cu.

Bell, Davies, and collaborators have pointed out that strong material-dependent effects may result from differences in target conductivity.[24,25] Conductivity has long been known to play an important role in shielding the resistive electrostatic field via a return current.[23] In our experiment, the return current also serves as the primary source of hot electrons, because the number of fast electrons we infer from our experiment is much greater than the number of electrons in a cubic laser spot size.

We have performed 1D LASNEX simulations[27] in which a high-energy Maxwellian distribution of electrons transport from the center of a solid-density sphere. The return current, heating, conductivity, and electrostatic fields are calculated self-consistently, and they show an ~40% loss of electron energy to resistive electrostatic fields. Other simulations have put this number at 30% (Ref. 25). This loss implies that our measurements of fast electrons place lower bounds on the original electron parameters, ideally requiring a correction for electrostatic effects.

However, electrostatic effects cannot fully explain the observed material dependence because η is not lowered by the same factor as E_0 in the different target materials. Another difference between the target materials is the underdense plasma that the ASE and prepulse form in front of the target. Our 2D calculations with LASNEX show a larger standoff between the critical and solid

densities in CH (40 μm), compared to Al (22 μm) and Cu (18 μm). The difference is due to the variation in the Z of the target, and it will affect the intensity distribution of the laser through filamentation instabilities and relativistic self-focusing.[18,19]

Summary

We have demonstrated a 20 to 30% conversion efficiency from laser energy into forward-propagated electrons in solid targets. The conversion efficiency seems to be a function of intensity, but not target material. A material dependence of electron temperature has been demonstrated for the first time at intensities greater than 10^{19} W/cm^2. Although this work will need to be extended to intensities of 10^{20} W/cm^2 to draw firmer conclusions on the feasibility of the fast ignitor fusion concept, this sizable conversion into forward-propagated electrons is an important validation for future research.

Acknowledgments

The authors would like to thank C. Brown, Y. Zakharenkov, J. Koch, and D. Pennington for their valuable contributions and assistance.

Notes and References

1. S. C. Wilks and W. L. Kruer, *IEEE J. Quant. Elec.* **33**, 1954 (1997).
2. M. Tabak et al., *Phys. Plasmas* **1**, 1626 (1994).
3. S. C. Wilks et al., *Phys. Rev. Lett.* **69**, 1383 (1992).
4. N. A. Ebrahim et al., *Phys. Rev. Lett.* **45**, 1179 (1980); F. Brunel, *Phys. Rev. Lett.* **59**, 52 (1987).
5. K. Estabrook and W. L. Kruer, *Phys. Fluids* **26**, 7 (1983).
6. F. Brunel, *Phys. Rev. Lett.* **59**, 52 (1987).
7. D. W. Forslund et al., *Phys. Rev. A* **11**, 670 (1975); G. J. Pert, *Plasma Phys.* **20**, 175 (1978); M. J. Everett et al., *Nature* **368**, 527 (1994); A. Modena et al., *Nature* **377**, 606 (1995).
8. J. D. Hares et al., *Phys. Rev. Lett.* **42,** 1216 (1979).
9. N. A. Ebrahim, C. Joshi, and H. A. Baldis, *Phys. Rev. A* **25**, 2440 (1982); B. Luther-Davies, A. Perry, and K. A. Nugent, *Phys. Rev. A* **35**, 4306 (1986).
10. H. Chen et al., *Phys. Rev. Lett.* **70**, 3431 (1993).
11. A. Rousse et al., *Phys. Rev. E* **50**, 2200 (1994).
12. Z. Jiang et al., *Phys. Plasmas* **2**, 1702 (1995).
13. U. Teubner et al., *Phys. Rev. E* **54**, 4167 (1996).
14. F. N. Beg et al., *Phys. Plasmas* **4**, 447 (1997).
15. G. Malka and J. L. Miquel, *Phys. Rev. Lett.* **77**, 75 (1996).
16. B. C. Stuart et al., *Optics Lett.* **22**, 242 (1997).
17. Y. Zakharenkov et al., *Rev. Sci. Instr.* **68**, 847 (1997).
18. C. E. Max et al., *Phys. Rev. Lett.* **33**, 209 (1974); P. Sprangle et al., *IEEE Trans. Plasma Sci.*, **PS-15**, 145 (1987); W. B. Mori et al., *Phys. Rev. Lett.* **60**, 1298 (1988).
19. A. Puhkov and J. Meyer-ter-Vehn, *Phys. Rev. Lett.* **76**, 3975 (1996).
20. J. Koch et al., *Lasers and Particle Beams* **16**, 225–232 (1998).
21. J. A. Halbleib and T. A. Mehlhorn, *Nucl. Sci. Engr.* **92**, 338 (1986).
22. M. G. Haines, *Phys. Rev. Lett.* **78**, 254 (1997).
23. D. J. Bond, J. D. Hares, and J. D. Kilkenny, *Phys. Rev. Lett.* **45**, 252 (1980).
24. A. R. Bell et al., *Plasma Phys. Control. Fusion* **39**, 653 (1997).
25. J. R. Davies et al., *Phys. Rev. E*, to be published.
26. A. P. Fews et al., *Opt. Commun.* **94**, 259 (1992).
27. G. B. Zimmerman and W. L. Kruer, *Comments Plasma Phys. Control. Fusion* **2**, 85 (1975).